Preparation of SnO_2 Nanoparticles Doped With Palladium and Graphene and Application for Ethanol Detection

Jiabin Fang, Yiping Zhu, Dajun Wu, Chi Zhang, Shaohui Xu, Dayuan Xiong, Pingxiong Yang, Lianwei Wang, and Paul K. Chu, *Fellow, IEEE*

***Abstract*— A novel ethanol gas sensor constructed with SnO_2 nanoparticles doped with palladium and graphene is described. By incorporating 0.1 wt% graphene and 3 wt% $PdCl_2$ into SnO_2, the working temperature of the sensor can be reduced to 40 °C and the response is 4.6. The operation temperature can be decreased to near room temperature due to the increased oxygen adsorption by palladium and the high electron mobility by graphene.**

***Index Terms*— Ethanol gas sensor, tin oxide, palladium, graphene.**

I. Introduction

ETHANOL is the main constituent in alcoholic drinks and excessive consumption which leads to slow reaction and judgment is one of the primary causes of traffic accidents [1], [2]. According to medical analyses, when the blood alcohol level is over the legal limit, the person's response will be impaired and traffic accidents may result [3]. In addition to education and public awareness, a convenient and sensitive ethanol sensor is crucial to legal enforcement and prevention of drunken driving.

As a multifunctional n-type semiconductor with a wide bandgap (E_g) of 3.6 eV, tin oxide (SnO_2) has been widely used in ethanol gas detection [4]. However, tin oxide gas sensors have a long recovery time and operate at a high temperature of usually more than 250 °C [3], [4] because the sensitive properties of tin oxide depend on the change in the surface resistance. In air, oxygen adsorbs onto the surface of tin oxide by the following reactions [5] to form oxygen anion and a space charge region:

$$\begin{aligned} O_{2(g)} &\leftrightarrow O_{2(ads)} \\ O_{2(ads)}+e^- &\leftrightarrow O^-_{2(ads)} \\ O^-_{2(ads)}+e^- &\leftrightarrow 2O^-_{(ads)} \\ O^-_{(ads)}+e^- &\leftrightarrow O^{2-}_{(ads)} \end{aligned}$$

With regard to pure tin oxide, the state of the ionized oxygen species is assumed to depend on the temperature. At a low temperature between 150 and 200 °C, oxygen adsorbs onto SnO_2 in a molecular form (as charged O- 2 ions) but at a temperature between 200 and 400 °C or higher, it dissociates into atomic oxygen (charged O^- or O^{2-}) [6]. O^- and O^{2-} play important roles in the detection of gaseous ethanol and so the sensor operates at a high temperature. As a result, this type of gas sensor requires an additional heating device and concomitant structure to provide the high temperature thereby increasing the hardware complexity. On the other hand, if the operating temperature can be reduced to room temperature, it is more convenient and compatible with the associated electronic circuitry enabling better integration with other sensors and chips. In order to overcome the shortcomings of tin oxide sensors, several strategies have been proposed, for example, producing nanostructured tin oxide including tin oxide quantum dots [7], [8], tin oxide nanowires [9], and tin oxide nanoflowers [4], doping with metals such as Pd [10] and Ag [11], and fabricating heterostructures such as SnO_2/TiO_2 [12], SnO_2/NiO [13], SnO_2/ZnO [5], [14]–[17], and others [18]–[20]. As emerging 2D nanomaterials, graphene has attracted much attention due to the large specific surface area, good chemical stability, and high carrier mobility [21]. In particular, reduced graphene oxide (rGO) has promising potential as an additive in gas sensing applications because of the high electron mobility at room temperature enabling operation at a lower temperature [21]–[23]. In addition, graphene oxide (GO), a derivative of graphene, can also be used in sensors due to its oxygen-containing functional groups [24], [25].

Addition of palladium can improve the response and reduce the effects of humidity on the gas sensitive properties [10] and graphene can reduce the working temperature [21].

Manuscript received June 22, 2017; revised August 16, 2017; accepted August 16, 2017. Date of publication August 21, 2017; date of current version September 8, 2017. This work was supported in part by the Shanghai Pujiang Program under Grant 14PJ1403600, in part by the National Natural Science Foundation of China under Grant 61176108, in part by PCSIRT, Huaian Applied Research, under Grant HAG2014034, in part by the Research Innovation Foundation of ECNU under Grant 78210245, in part by the Scientific Research Foundation for the Returned Overseas Chinese Scholars, State Education Ministry, in part by the Science and Technology Commission of Shanghai Municipality under Grant 14DZ2260800, in part by the Open Research Fund of Shanghai Key Laboratory of Multidimensional Information Processing, East China Normal University, and in part by the City University of Hong Kong Applied Research Grant under Grant 9667104 and Grant 9667122. The associate editor coordinating the review of this paper and approving it for publication was Prof. Zeynep Celik-Butler. *(Corresponding author: Yiping Zhu.)*

J. Fang, Y. Zhu, D. Wu, C. Zhang, S. Xu, D. Xiong, P. Yang, and L. Wang are with the Key Laboratory of Polar Materials and Devices, Ministry of Education, Shanghai Key Laboratory of Multidimensional Information Processing, East China Normal University, Shanghai 200241, China, and also with the Department of Electronic Engineering, East China Normal University, Shanghai 200241, China (e-mail: ypzhu@ee.ecnu.edu.cn).

P. K. Chu is with the Department of Physics and Department of Materials Science and Engineering, City University of Hong Kong, Hong Kong.

Digital Object Identifier 10.1109/JSEN.2017.2742583

TABLE I
SAMPLE DETAILS

Sample Name	$PdCl_2$	rGO
S1	none	none
S2	3 wt%	none
S3	3 wt%	0.1 wt%
S4	3 wt%	0.5 wt%
S5	3 wt%	1 wt%

However, to our knowledge, the synergistic effects of palladium and graphene pertaining to tin oxide sensor have not been reported. In this work, tin oxide nanoparticles synthesized by a simple precipitation method are doped with palladium and graphene to produce a gas sensor that operates at a relatively low temperature and the ethanol sensing performance is evaluated systematically.

II. EXPERIMENTAL DETAILS

All the chemicals were analytical grade and used without further purification. $SnCl_4 \cdot 5H_2O$ was added to deionized water to form a 0.5 M aqueous solution and a small amount of citric acid was added to prevent the formation of sediment by $SnCl_4$ hydrolysis. Ammonium hydroxide was introduced to the solution slowly under stirring to obtain the precipitate. The tin hydroxide precipitate was centrifuged at 6000 rpm three times and 9000 rpm three times and then rinsed with deionized water and absolute ethanol thrice. The precipitate was pulverized and the tin hydroxide powder was sintered for 2 hours at 600 °C to obtain the tin oxide powder. The graphite oxide was synthesized from natural graphite by Hummer's method and the rGO was obtained by pyrolyzing graphite oxide at 1000 °C under Ar [26].

The pure tin oxide powder was labeled S1. After adding tin dioxide powder and 3 wt% palladium chloride into an adequate amount of deionized water, it was stirred and dried to form the powder designated as S2. By using the same method, SnO_2 samples with 3 wt% $PdCl_2$ and 0.1 wt%, 0.5 wt%, or 1 wt% of rGO were prepared and labeled as S3, S4 and S5, respectively, as shown in Table I.

The powder was added to a small amount of deionized water to form a paste. The paste was coated on a ceramic tube and dried at 100 °C for 12 h. The tube was then welded to a six pin base to form a gas sensor that was aged at 65 °C for 48 h.

The gas sensing performance was assessed on a CGS-8 gas-sensing system. The air was directly collected from the cleanroom. The temperature of the cleanroom was 22 °C and the humidity was control to be 40 %rh. Gaseous ethanol was injected into a chamber by a clean syringe and the concentration was adjusted by controlling the injected amount. The response was defined as R_a/R_g, where R_a represented the resistance in air and R_g was the resistance in gaseous ethanol. The response time was defined as the time required to reach 90% of the reduced resistance and the recovery time was defined as the time required to reach 90% of the initial resistance [5].

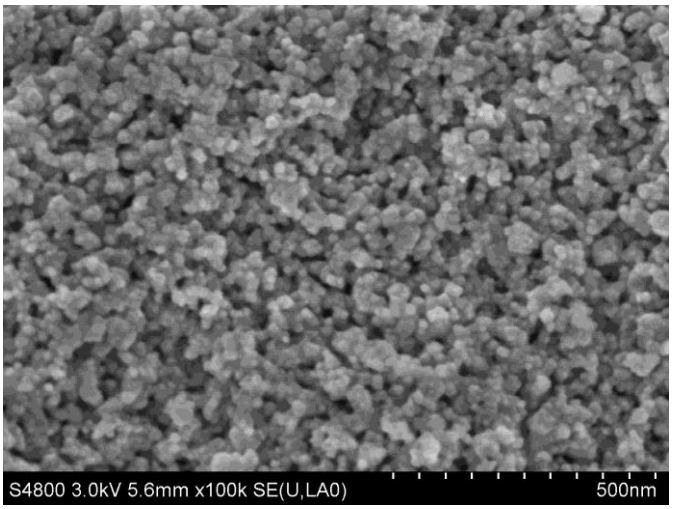

Fig. 1. SEM image of sintered SnO_2 nanoparticles.

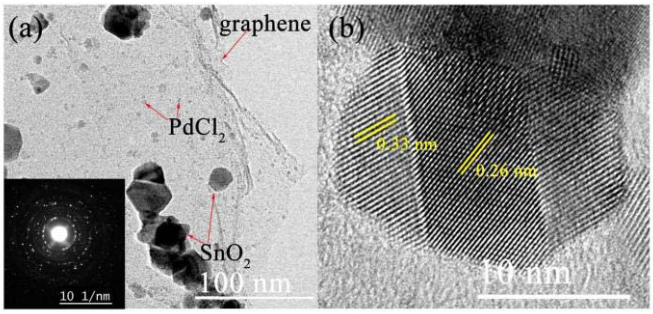

Fig. 2. TEM image of SnO_2 doped with $PdCl_2$ and graphene (a) at low magnification, (b) at high magnification.

III. RESULT AND DISCUSSION

The scanning electron microscopy (SEM) images of the tin oxide nanoparticles is shown in Figure 1. The nano-scale particles with an individual size of 10-20 nm interconnect with each other to form a porous surface which is expected to promote gas adsorption due to the larger specific surface area and consequently the gas-sensing properties of the device.

Figure 2(a) shows the morphology of the SnO_2 doped with $PdCl_2$ and graphene. The size of the nano-scale tin oxide particles is similar to that shown in the SEM image and the size of graphene is measured in microns. The palladium chloride particles have the nanoscale and some of them are scattered on graphene and the others are attached on the surface of tin oxide. Figure 2(b) shows the image of tin oxide particles at high magnification. Tin oxide belongs to the rutile structure and SnO_2 (110) with the 0.33 nm lattice spacing and SnO_2 (101) with the 0.26 nm lattice spacing are observed.

Figure 3 depicts the X-ray diffraction (XRD) patterns of the powders. The XRD spectra show (110), (101), (200), and (211) SnO_2 peaks (2θ) at 26.78^o, 34.24^o, 38.24^o, and 52.14^o, respectively. Tin oxide has a polycrystalline structure corresponding to the SnO_2 tetragonal rutile phase (ICDD n.00-041-1445).

The Raman patterns of the samples are shown in Figure 4 and there is a clear tin oxide peak at 632 cm^{-1}. The samples with added palladium chloride show the peak at

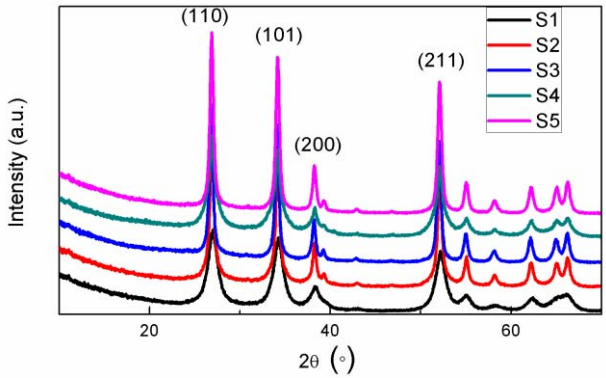

Fig. 3. XRD patterns of the samples.

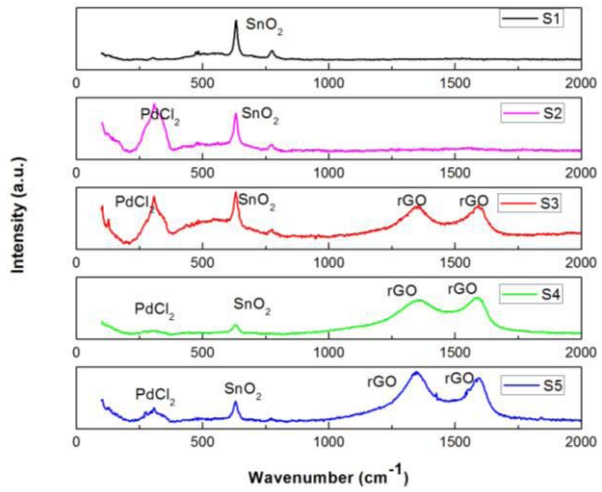

Fig. 4. Raman patterns of the samples.

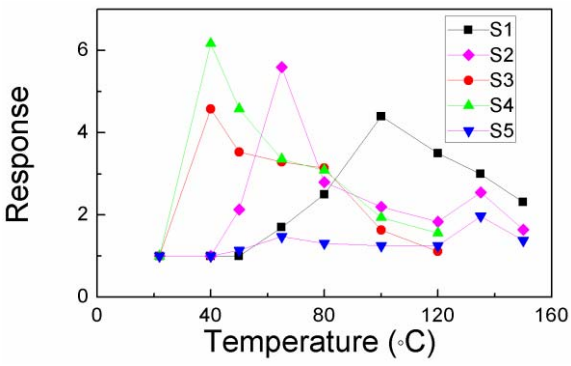

Fig. 5. Response (R_a/R_g) of the samples towards 100 ppm gaseous ethanol at various operation temperature.

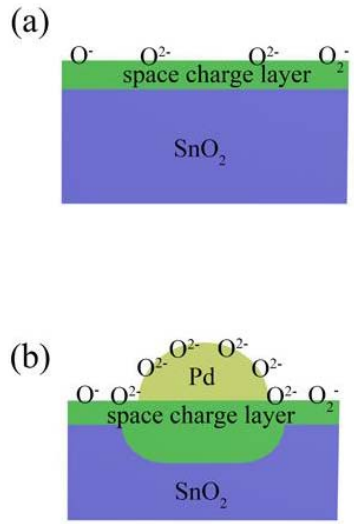

Fig. 6. (a) Oxygen ions on pure SnO_2. (b) Oxygen ions on the sample with Pd.

around 300 cm^{-1}. Similarly, the samples with added graphene exhibit peaks at 1350 cm^{-1} and 1600 cm^{-1}. The Raman patterns show successful incorporation of palladium chloride and graphene into the SnO_2 powder.

Figure 5 shows the response to 100 ppm gaseous ethanol at different temperature. Pure tin oxide shows the best response of 4.4 at 100 °C and that of S2, S3, and S4 is 5.8, 4.6, and 6.2 at 65 °C, 40 °C, and 40 °C, respectively. The working temperature of S2 is lower than that of S1 and that of S3 or S4 is even lower. The result shows that adding palladium chloride and graphene can reduce the operating temperature of the sensor. However, no sample can detect ethanol without heating at 22 °C. It is also found that the response of S5 is poor. The initial resistance of S5 is much smaller than that of other samples because too much graphene reduces the resistance making the change difficult to monitor.

Compared to pure tin oxide, the sample mixed with 3wt% $PdCl_2$ shows better response at a lower temperature. The samples with graphene operate at an even lower temperature, but the response is poor when the mass ratio of graphene is 1 wt%.

When palladium is present in tin oxide, more oxygen ions are formed on the surface because oxygen adsorbs onto the metal ions easily forming O^{2-} [10] as shown in Figure 6. Consequently, the number of electrons decreases, the space charge region expands, and the initial resistance increases. On the other hand, more electrons can be reclaimed in gaseous ethanol and hence, the response increases. At the same time, since it is easier to adsorb oxygen ions, there are enough oxygen ions even at a lower temperature and the operation temperature can be reduced. Doping with graphene has been reported to decrease the working temperature [21] because of the oxygen adsorption ability and high electron mobility of rGO at room temperature.

Figure 7 depicts the response curve of sample S3 and S4 at 40 °C in the presence of 100 ppm gaseous ethanol. The response time of S3 and S4 is 93s and 56s and the recovery time is 130s and 113s, respectively. This shows that more rGO improves the response and recovery more under certain conditions.

Owing to adsorbed oxygen anions on the SnO_2 surface, the surface energy band level rises forming a barrier between crystalline grains. Electrons cannot easily move among grains because they should overcome these barriers. Hence, the resistance cannot decrease or recovery quickly. It is possible to shorten the response time and recovery time because rGO has high electron mobility at a low temperature. The "highway band" constructed by rGO is more effective than the "rough road band" constituted by crystalline grains as illustrated

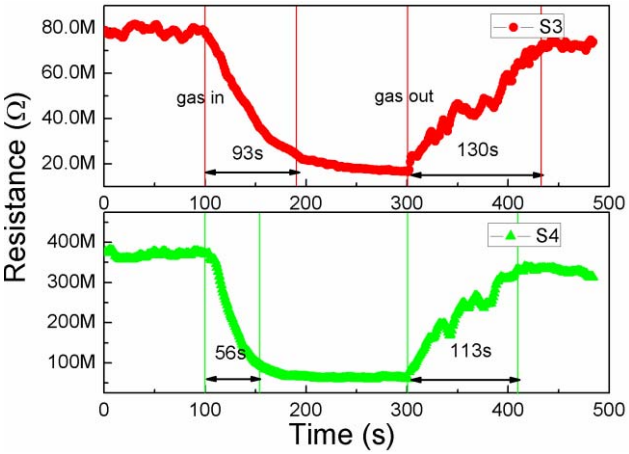

Fig. 7. Dynamic ethanol sensing transient of the two sensors towards 100 ppm ethanol at 40 °C.

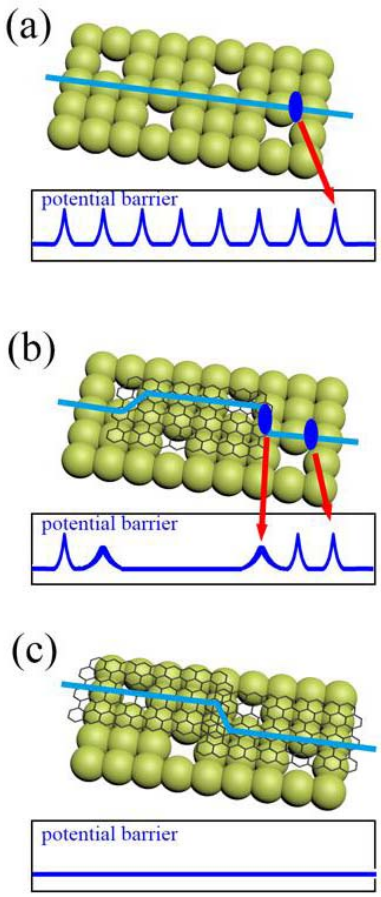

Fig. 8. (a) Sample without rGO. (b) Sample with a small amount of rGO. (c) Sample with a large amount of rGO.

in Figure 8. Without rGO as shown in Figure 8(a), electrons must overcome the high potential barriers to move among individual SnO_2 nanoparticles [12] but in the "highway band" constructed with rGO, carrier transport is more efficient as shown in Figure 8(b) giving rise to more rapid response and recovery. However, if the amount of rGO is excessive, a conducting path composed of rGO is created as shown in Figure 8(c) and electrons only migrate on rGO. The initial resistance is thus quite small leading to poor sensitivity similar to that observed from sample S5 as shown in Figure 5.

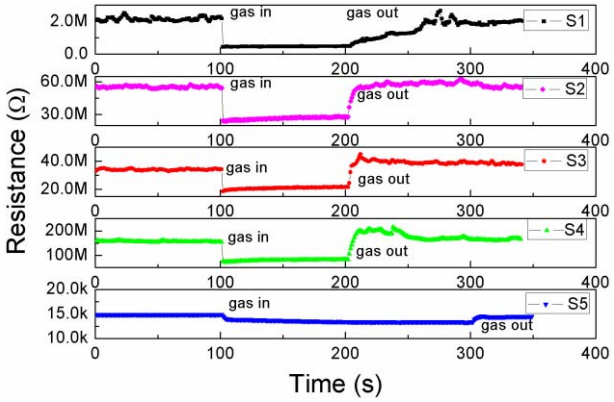

Fig. 9. Dynamic ethanol sensing transient of the sensors towards 100 ppm ethanol at 100 °C.

Figure 9 shows the dynamic ethanol sensing trends of the sensors towards 100 ppm gaseous ethanol at 100 °C. The recovery time of S2, S3, and S4 is reduced greatly compared to S1. At the same time, the response time and recovery time are reduced at the higher temperature compared to Figure 7. This is because electrons can move faster at a higher temperature to expedite the related reaction. Consequently, the response time and recovery time are reduced significantly. Besides, although S5 shows good recovery characteristics, the response is very small. There are several peaks in the resistance curve after exposure to air again and they can sometimes be slightly larger than the initial resistance. It is because the temperature changes only slightly as a result of gas convection during exposure to air.

On account of the change in the adsorption capacity caused by $PdCl_2$and rGO, there is big difference in the initial resistance among the samples. Furthermore, the gas sensing properties depend on the amount of graphene. As for the sample with 0.1 wt% rGO, the change in oxygen adsorption is negligible because the amount of rGO is very small and the initial resistance of S2 is close to the initial resistance of S3. The resistance of the 1 wt% graphene sample is reduced because the "highway band" decreases the resistance and this effect overwhelms the impact by the resistance increase from adsorption. It should be noted that the initial resistance of S4 sample is accidentally increased because of the uneven thickness of the powder caused by manual smearing. Nevertheless, we focus on the response (R_a/R_g) instead of R_a and so the nonuniformity due to manual smearing does not matter a great deal.

All in all, S3 and S4 deliver better sensing performance and our results show that the amount of rGO should be less than 1 wt% in order to achieve good sensitivity.

Figure 10 shows the repeatability of S3 and S4 at 40 °C in the presence of 100 ppm gaseous ethanol. The resistance of S4 decreases compared to the initial resistance with cycling. Under normal circumstances, the following reactions occur in the gaseous ethanol [5]:

$$CH_3CH_2OH + 6O^-_{(ads)} \rightarrow 2CO_2 + 3H_2O + 6e^-$$
$$CH_3CH_2OH + 6O^{2-}_{(ads)} \rightarrow 2CO_2 + 3H_2O + 12e^-$$

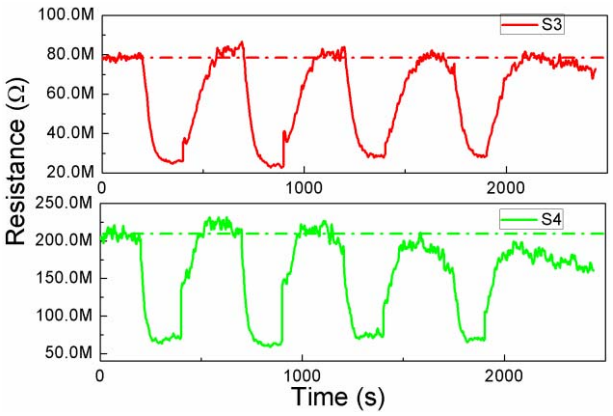

Fig. 10. Repeatability of S3 and S4 at 40 °C in the presence of 100 ppm gaseous ethanol.

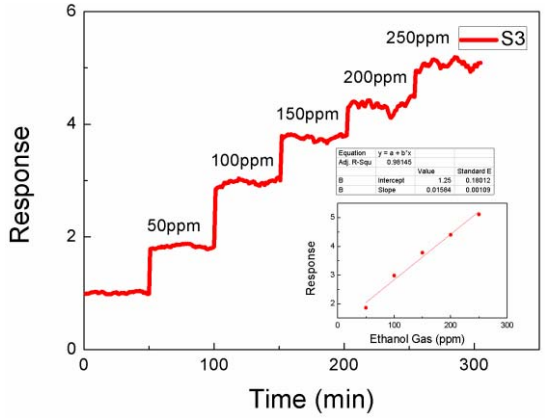

Fig. 11. Dynamic ethanol sensing transient of S3 towards various gaseous ethanol at 40 °C and the gas response as a function of ethanol concentration.

Tin oxide reclaims the electrons to reduce the resistance but at a low temperature, the intermediate products of the reaction adsorb on rGO as shown in the following [27]:

$$CH_3CH_2OH + O^- \rightarrow CH_3CHO + H_2O + e^-$$
$$CH_3CHO + O^- \rightarrow CH_3COOH + e^-$$

The intermediate products may not be converted to CO_2 and be absorbed by rGO on the surface at the low temperature. Therefore, the resistance cannot be fully recovered to the initial value at 40 °C. Since S4 has more graphene, the amount of adsorbed intermediate products is larger and the resistance is reduced significantly. As the test proceeds, the response is slightly smaller than the highest response of the device perhaps because a part of rGO is consumed in the test, especially at a high temperature.

Comparing to other samples, S3 containing 3 wt% $PdCl_2$ and 0.1 wt% rGO can be operated at 40 °C and shows rapid response and recovery characteristics as well as good stability during repeated use. Figure 11 shows the dynamic ethanol sensing trend of S3 in the presence of different concentrations of gaseous ethanol at 40 °C and good linearity is revealed. The relationship between the ethanol concentration and response can be described as:

$$y = 1.25 + 0.01584x \quad (1)$$

where y represents the response and x is the ethanol gas concentration. The linearity is 98.1%. The results demonstrate that SnO_2 nanoparticles mixed with 0.1 wt% rGO and 3 wt% $PdCl_2$ can deliver good gaseous ethanol sensing performance at a low temperature and 40%rh.

IV. Conclusion

The sensor made of SnO_2 mixed with 3 wt % $PdCl_2$ and 0.1 wt% rGO shows the best response to gaseous ethanol such as a response time of 93 s and recovery time of 130 s at 40 °C and 40%rh. This sensor which can be operated at near room temperature has a wider range of applications compared to sensors that only work at a high temperature. The synergistic effects of palladium and graphene exploited in this sensor design are more effective compared to that with only palladium. The amount of rGO is found to affect the sensing properties.

References

[1] S. Basu, Y.-H. Wang, C. Ghanshyam, and P. Kapur, "Fast response time alcohol gas sensor using nanocrystalline F-doped SnO_2 films derived via sol–gel method," *Bull. Mater. Sci.*, vol. 36, no. 4, pp. 521–533, 2013.

[2] E. Comini, G. Faglia, G. Sberveglieri, Z. Pan, and Z. L. Wang, "Stable and highly sensitive gas sensors based on semiconducting oxide nanobelts," *Appl. Phys. Lett.*, vol. 81, no. 10, pp. 1869–1871, 2002.

[3] J.-J. Ho *et al.*, "High sensitivity ethanol gas sensor integrated with a solid-state heater and thermal isolation improvement structure for legal drink-drive limit detecting," *Sens. Actuators B, Chem.*, vol. 50, no. 3, pp. 227–233, 1998.

[4] W. X. Jin *et al.*, "Synthesis of hierarchical SnO_2 nanoflowers with enhanced acetic acid gas sensing properties," *Appl. Surf. Sci.*, vol. 353, pp. 71–78, Oct. 2015.

[5] S. H. Yan *et al.*, "Synthesis of SnO_2–ZnO heterostructured nanofibers for enhanced ethanol gas-sensing performance," *Sens. Actuators B, Chem.*, vol. 221, pp. 88–95, Dec. 2015.

[6] A. Gurlo, "Interplay between O_2 and SnO_2: Oxygen ionosorption and spectroscopic evidence for adsorbed oxygen," *ChemPhysChem*, vol. 7, pp. 2041–2052, Oct. 2006.

[7] Y. He, P. Li, J. Li, J. Zhang, F. Fan, and D. Li, "Ultrafast response and recovery ethanol sensor based on SnO_2 quantum dots," *Mater. Lett.*, vol. 165, pp. 50–54, Feb. 2016.

[8] J. S. Tawale, G. Gupta, A. Mohan, A. Kumar, and A. K. Srivastava, "Growth of thermally evaporated SnO_2 nanostructures for optical and humidity sensing application," *Sens. Actuators B, Chem.*, vol. 201, pp. 369–377, Oct. 2014.

[9] I. Castro-Hurtado, J. Herrán, G. Ga Mandayo, and E. Castaño, "SnO_2-nanowires grown by catalytic oxidation of tin sputtered thin films for formaldehyde detection," *Thin Solid Films*, vol. 520, no. 14, pp. 4792–4796, 2012.

[10] N. Ma, K. Suematsu, M. Yuasa, T. Kida, and K. Shimanoe, "Effect of water vapor on Pd-loaded SnO_2 nanoparticles gas sensor," *Appl. Mater. Inter.*, vol. 7, no. 10, pp. 5863–5869, 2015.

[11] H. Kim, C.-S. Park, K.-M. Kang, M.-H. Hong, Y.-J. Choi, and H.-H. Park, "The CO gas sensing properties of direct-patternable SnO_2 films containing graphene or Ag nanoparticles," *New J. Chem*, vol. 39, no. 3, pp. 2256–2260, 2015.

[12] X. Wang, Y. Sang, D. Wang, S. Ji, and H. Liu, "Enhanced gas sensing property of SnO_2 nanoparticles by constructing the SnO_2-TiO_2 nanobelt heterostructure," *J. Alloys Compounds*, vol. 639, pp. 571–576, Aug. 2015.

[13] D. Ju *et al.*, "High triethylamine-sensing properties of NiO/SnO_2 hollow sphere P–N heterojunction sensors," *Sens. Actuators B, Chem.*, vol. 215, pp. 39–44, Aug. 2015.

[14] H. W. Kim, H. G. Na, Y. J. Kwon, H. Y. Cho, and C. Lee, "Decoration of Co nanoparticles on ZnO-branched SnO_2 nanowires to enhance gas sensing," *Sens. Actuators B, Chem.*, vol. 219, pp. 22–29, Nov. 2015.

[15] G. Sun *et al.*, "Synthesis and enhanced gas sensing properties of flower-like SnO_2 hierarchical structures decorated with discrete ZnO nanoparticles," *J. Alloys Compounds*, vol. 617, pp. 192–199, Dec. 2014.

[16] W. Tang, J. Wang, P. Yao, and X. Li, "Hollow hierarchical SnO_2-ZnO composite nanofibers with heterostructure based on electrospinning method for detecting methanol," *Sens. Actuators B, Chem.*, vol. 192, pp. 543–549, Mar. 2014.
[17] B. Zhang *et al.*, "Actinomorphic ZnO/SnO_2 core–shell nanorods: Two-step synthesis and enhanced ethanol sensing propertied," *Mater. Lett.*, vol. 160, pp. 227–230, Dec. 2015.
[18] L. Geng, Y. Zhao, X. Huang, S. Wang, S. Zhang, and S. Wu, "Characterization and gas sensitivity study of polyaniline/SnO_2 hybrid material prepared by hydrothermal route," *Sens. Actuators B, Chem.*, vol. 120, pp. 568–572, Jan. 2007.
[19] A. Shanmugasundaram, P. Basak, L. Satyanarayana, and V. Sunkara Manorama, "Hierarchical SnO/SnO_2 nanocomposites: Formation of *in situ* $p-n$ junctions and enhanced H_2 sensing," *Sens. Actuators B, Chem.*, vol. 185, pp. 265–273, Aug. 2013.
[20] A. Sharma, M. Tomar, and V. Gupta, "WO3 nanoclusters–SnO_2 film gas sensor heterostructure with enhanced response for NO_2," *Sens. Actuators B, Chem.*, vol. 176, pp. 675–684, Jan. 2013.
[21] D. Zhang, A. Liu, H. Chang, and B. Xia, "Room-temperature high-performance acetone gas sensor based on hydrothermal synthesized SnO_2-reduced graphene oxide hybrid composite," *RSC Adv.*, vol. 5, no. 4, pp. 3016–3022, 2015.
[22] K. Inyawiler, A. Wisitsoraat, C. Sriprachaubwong, A. Tuantranont, S. Phanichphant, and C. Liewhiran, "Rapid ethanol sensor based on electrolytically-exfoliated graphene-loaded flame-made In-doped SnO_2 composite film," *Sens. Actuators B, Chem.*, vol. 209, pp. 40–55, Mar. 2015.
[23] Z. Wang, Y. Zhang, S. Liu, and T. Zhang, "Preparation of Ag nanoparticles-SnO_2 nanoparticles-reduced graphene oxide hybrids and their application for detection of NO_2 at room temperature," *Sens. Actuators B, Chem.*, vol. 222, pp. 893–903, Jan. 2016.
[24] S. Erogul, S. Z. Bas, M. Ozmen, and S. Yildiz, "A new electrochemical sensor based on Fe_3O_4 functionalized graphene oxide-gold nanoparticle composite film for simultaneous determination of catechol and hydroquinone," *Electrochim. Acta*, vol. 186, pp. 302–313, Dec. 2015.
[25] Y. Acikbas, S. Z. Bas, M. Ozmen, R. Capan, and M. Erdogan, "Optical properties and swelling behavior of Fe_3O_4 functionalized graphene oxide composite thin film," *IEEE Sensors J.*, vol. 17, no. 5, pp. 1222–1229, Mar. 2017.
[26] W. S. Hummers, Jr., and R. E. Offeman, "Preparation of graphitic oxide," *J. Amer. Chem. Soc.*, vol. 80, no. 6, p. 1339, 1958.
[27] Y. Qu, H. Wang, H. Chen, M. Han, and Z. Lin, "Characterization and sensing properties of mesoporous C/SnO_2 nanocomposite," *Sens. Actuators B, Chem.*, vol. 228, pp. 595–604, Jun. 2016.

Jiabin Fang received the B.S. degree in electronic science and technology from East China Normal University in 2014, where he is currently pursuing the master's degree with the Department of Electrical Engineering. His research focuses on the semiconducting metal oxide thin films and gas sensors.

Yiping Zhu received the B.S. degree in information engineering from Shanghai Jiao Tong University in 2002, and the Ph.D. degree in electronic science and technology from Tsinghua University in 2007. From 2008 to 2009, he was a Post-Doctoral Research Associate with the University of Florida. From 2009 to 2012, he was a Post-Doctoral Scholar with the University of California, Berkeley. He joined the faculty of East China Normal University in 2012, where he is currently an Associate Professor with the Department of Electronic Engineering. His research interests include microfabrication technology, MEMS, and micro-sensors and actuators.

Dajun Wu is currently pursuing the Ph.D. degree with the Department of Electrical Engineering, East China Normal University. His doctoral research focuses on the development of carbon-based materials and macroporous and electrically conductive network for energy storage devices and field emission devices, such as supercapacitors, batteries, and electron sources, including the design and synthesization of nanocomposites.

Chi Zhang is currently pursuing the Ph.D. degree with the Department of Electronic Engineering, East China Normal University. Her doctoral research focuses on the MEMS process and sensors, such as electric field emission devices and gas sensors.

Shaohui Xu received the Ph.D. degree from the Surface Physics Laboratory (National Key Laboratory), Fudan University, in 2003. He joined the faculty of the Department of Electrical and Engineering, East China Normal University. His current research focuses mainly on MEMS and nanomaterials for energy-related applications, including thermoelectric devices, batteries, and supercapacitors.

Dayuan Xiong received the Ph.D. degree from the Chinese Academy of Sciences in 2007. He joined the faculty of the School of Information Science Technology, East China Normal University. His recent research interests include optoelectronics, novel sensor technology, and material/device for energy storage.

Pingxiong Yang received the Ph.D. degree from the Shanghai Institute of Metallurgy, Chinese Academy of Sciences, in 1997. He is currently a Professor with the Department of Electrical Engineering, East China Normal University. His research interests include new energy material and devices.

Lianwei Wang received the master's degree from the Department of Physics, Nanjing University, in 1992, and the Ph.D. degree from the Shanghai Institute of Metallurgy, Chinese Academy of Sciences, China, in 1995. From 1995 to 2000, he was with the Institute of Metallurgy, Chinese Academy of Sciences of China. From 2001 to 2003, he held a post-doctoral position with the Delft University of Technology, The Netherlands. Since 2003, he has been a Professor with East China Normal University. His current research interests include micro-sensors and solar cell, and microfabrication technology.

Paul K. Chu received the Ph.D. degree in chemistry from Cornell University. He is currently the Chair Professor of Materials Engineering with the City University of Hong Kong. His research interests are quite diverse covering plasma and surface engineering as well as different types of functional materials. He is a Fellow of the Hong Kong Academy of Engineering Sciences, the American Physical Society, the American Vacuum Society, the Institute of Electrical and Electronics Engineers (IEEE), the Materials Research Society, and the Hong Kong Institution of Engineers. He is a Supervising Senior Editor of the IEEE TRANSACTIONS ON PLASMA SCIENCE and an Associate Editor of *Materials Science and Engineering Reports*.